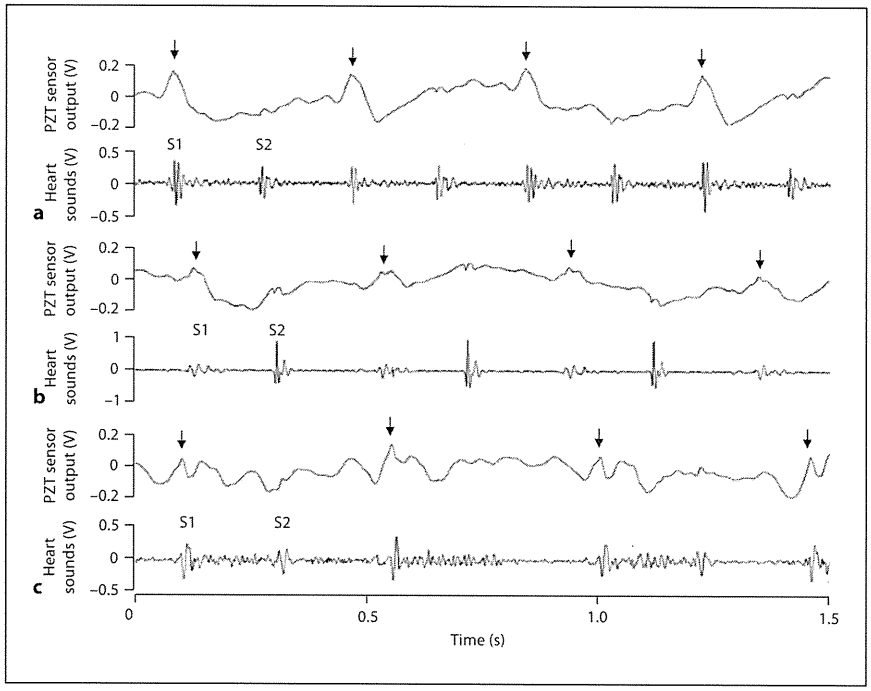

Fig. 2. PZT sensor output (upper) and filtered and amplified heart sounds (lower) with normal shape (**a**), accentuated second sounds (**b**) and heart murmurs (**c**) recorded in the preliminary study. Low frequency components of S_1 (arrows) were detected in the PZT sensor outputs, which are likely to indicate gross heart movement and have different waveforms between the three traces.

Data Recording

The PZT sensor was fixed with an adhesive plaster to a towel-covered foam mattress in an incubator and covered with a folded face towel, on which the neonate was placed; therefore, there were 2 layers of towel cloth between the PZT sensor and the back (or chest/abdomen) of the neonate (fig. 1). Adhesive ECG electrodes were also attached to the chest or back of a neonate for ECG/IPG. In addition, other catheters, tubes or sensors (orogastric tube, percutaneous central venous catheter, oxygen saturation monitor) were used for all neonates, while an orotracheal tube, transcutaneous CO_2 monitor and umbilical arterial/venous catheter were additionally used for serious cases. After placing the PZT sensor under a neonate, a physician or nurse corrected the neonate's position as usual during their routine work, but no attention was paid to the PZT sensor setting during the measurement. In addition, the sleeping position of all neonates was routinely changed at every 3 h into either supine, prone, right or left (side down) lateral position.

PZT sensor output and ECG signal output from a patient monitor (DS-5100E; Fukuda Denshi, Japan) were uploaded to a computer installed with data acquisition software (Axoscope9; Molecular Devices, USA) via a 2-channel A/D converter. Another data recording system (Acquisition 2.0; Unique Medical) was used for three-channel recording including respiratory signal of IPG in addition to the above signals. Heart sounds, breathing movement signals and other digital outputs of the PZT system were not recorded so as to maintain data less than ~1 Gbyte; data were sampled at 2-millisecond intervals to give a maximum file size for continuous recordings over 3 days of ~1 Gbyte. Measurement for each neonate was started at 0 (median, range 0–8) days and continued for 1–9 days. In the preliminary study, PZT sensor output and ECG signal were recorded for 5–10 min by a data recorder (PC204Ax; Sony, Japan) at a sampling rate of 20 kHz to analyze the heart sound waveform (fig. 2).

Brief Assessment of Inherent Performance of the PZT Sensor

Inherent performance of the PZT sensor was assessed using data analysis software (Clampfit 9.2; Molecular Devices), which is often used to analyze the firing rate of spontaneously firing cells, and a spreadsheet application (Excel; Microsoft, USA) after data recording. Firstly, the PZT sensor output signal was filtered (high-pass 70 Hz: 8-pole Bessel) by a filter of the data analysis software to extract heart sounds. Secondly, heart sounds and ECG signals for 1 min each were extracted from periods when no large noise, fluctuation, arrhythmia and apnea occurred. Thirdly, the peak time data of every first sound (S_1) and second sound (S_2) in the heart sound signal were then automatically sampled by template search analysis (a type of pattern recognition processing) of the data analysis software, which searches the whole record for similar signals with a predefined representative S_1 epoch regardless of their amplitude. Then, using the spreadsheet application, S_1–S_1 intervals were compared with corresponding R–R intervals, which were similarly obtained from the ECG by template search analysis after a filtering process (high-pass >5 Hz). S_1–S_1 interval errors arising from multi-peaks of the S_1 signal [7] were manually corrected. Twenty-seven neonates (19 boys and 8 girls; GA 34.5 ± 3.5 weeks, BW 2,027 ± 800 g) were recruited for this assessment (table 1). Similarly, respiration signals obtained by the PZT sensor and IPG for 1 min each were extracted and band-pass filtered (0.5–0.6 and 0.5–0.8 Hz, respectively) to obtain the breathing intervals of 11 newborn infants (5 boys and 6 girls; GA 35.0 ± 3.6

Table 1. Clinical characteristics of patients enrolled in long and short period assessments of heart rate and breathing rate detection by the PZT sensor and those in body motility assessment in 2 groups that underwent ECG recording with and without the PZT sensor measurement

	Long and short period assessments		Body motility assessment	
	heart rate (n = 27)	breathing rate (n = 11)	ECG + PZT sensor (n =10)	ECG only (n = 10)
Age at measurement, days	0 [0–3]	1 [0–5]	1 [0–5]	0 [0–3]
Gestational age at birth, weeks	34.9 [25.3–39.9]	35.0 [28.6–41.1]	34.0 [28.6–40.7]	35.2 [32.3–40]
Boys	19 (70)	5 (45)	5 (50)	6 (60)
Neonatal weight, g	1,960 [742–4,126]	2,157 [1,117–3,316]	2,152 [1,117–2,852]	2,029 [1,302–2,434]
ELBW	2 (7.4)	0 (0)	0 (0)	0 (0)
VLBW	5 (18.5)	2 (18.2)	2 (20)	2 (20)
LBW	14 (51.9)	6 (54.5)	6 (60)	8 (80)
Diagnosis				
Amniotic infection	1 (3.7)	0 (0)	0 (0)	0 (0)
Anal atresia	1 (3.7)	0 (0)	0 (0)	0 (0)
Asphyxia	1 (3.7)	0 (0)	0 (0)	0 (0)
Asphyxia neonatorum	1 (3.7)	0 (0)	0 (0)	0 (0)
Atrial septal defect	1 (3.7)	0 (0)	0 (0)	0 (0)
Chromosome abnormality	1 (3.7)	0 (0)	0 (0)	0 (0)
Cleft of the soft palate	0 (0)	1 (9.1)	0 (0)	0 (0)
Down syndrome	2 (7.4)	0 (0)	0 (0)	0 (0)
Duodenal atresia	1 (3.7)	0 (0)	0 (0)	0 (0)
Patent ductus arteriosus	2 (7.4)	1 (9.1)	1 (10)	0 (0)
Patent foramen ovale	1 (3.7)	0 (0)	0 (0)	0 (0)
Peripheral pulmonary stenosis	1 (3.7)	0 (0)	0 (0)	0 (0)
Pierre Robin sequence	0 (0)	1 (3.7)	0 (0)	0 (0)
Pneumothorax	1 (3.7)	0 (0)	0 (0)	0 (0)
Respiratory distress syndrome	3 (11.1)	0 (0)	0 (0)	0 (0)
Transient tachypnea of the newborn	2 (7.4)	1 (9.1)	1 (10)	0 (0)
Transient myeloproliferative disease	2 (7.4)	0 (0)	0 (0)	0 (0)
Ventriculomegaly	0 (0)	1 (9.1)	1 (10)	0 (0)
Mechanical ventilation				
Nasal continuous positive airway pressure	3 (11.1)	0 (0)	0 (0)	0 (0)
Intermittent mandatory ventilation	2 (7.4)	0 (0)	0 (0)	0 (0)
High frequency oscillation	2 (7.4)	1 (9.1)	1 (10)	0 (0)

Data are expressed as medians with ranges in square brackets or numbers with percentages in parentheses.

weeks, BW 2,150 ± 650 g) by template search analysis to compare the breathing interval between the two methods. These comparisons of cardiac and breathing intervals during a short period were finally evaluated by the correlation coefficient and Bland-Altman plot using a spreadsheet application.

Assessment of PZT Sensor Measurement of a Long Duration

Long-term assessment was unavoidably simplified because the manual verification/correction of 1-min PZT data took 2 h and a 1-week data set would take ~10 years. However, the manual verification of data was not completely abandoned but we verified data as much as possible, searching for errors by observing HR/BR trend graphs and reanalyzing the periods with vertical lines (fig. 3), which indicate false positives/negatives or noises, by changing threshold and template for template search analysis or by measuring signal peaks manually.

Detection rates of HR and BR during >10 h (9 days maximum) long measurement by the PZT system and ECG/IPG were evaluated according to the total time during which cardiac beats and respiratory activity were identified by template search analysis. For the evaluation, raw data were divided into 24-hour records. The divided data were then subjected to template search analysis to obtain a series of S_1 and S_2 time peaks and peaks of R waves after high-pass filtering of 70 and 5 Hz, respectively. These peak time data were used to calculate instantaneous HR using a spreadsheet application; HRs between 100 and 380 (beats/min) were scored as correct because detecting the S_1–S_2 or S_2–S_1 interval doubled the HR (fig. 3a, upper), while an acceptable cardiac inter-

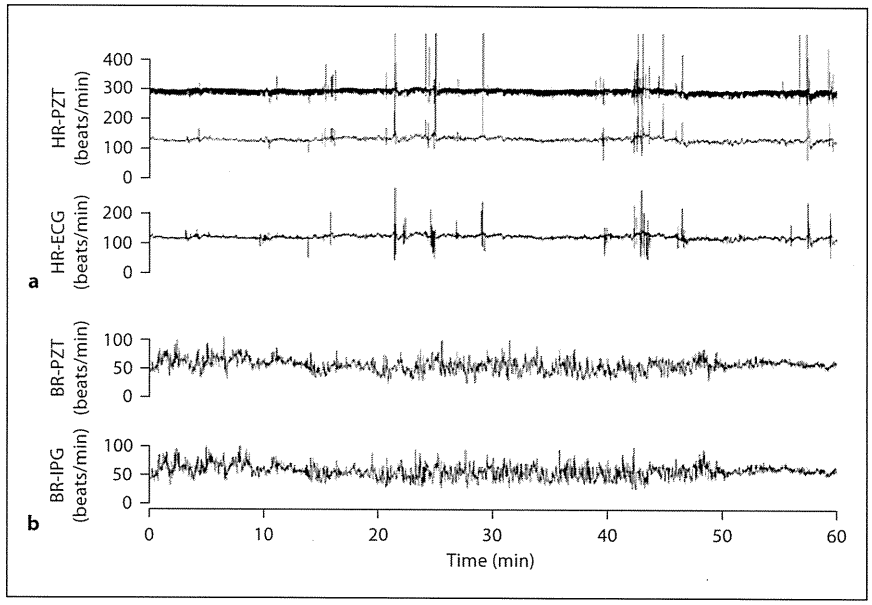

Fig. 3. Time courses of HR and BR for 1 h measured by the PZT sensor system and ECG/IPG. **a** Instantaneous HR detected by the PZT sensor system (HR-PZT: upper) and that by ECG (HR-ECG: lower). HR-PZT has 2 traces: the upper trace indicates doubled HR calculated from S_1–S_2 and S_2–S_1 intervals; the lower trace indicates HR calculated from S_1–S_1 [= (S_1–S_2) + (S_2–S_1)] intervals. HRs detected by the PZT sensor and ECG were in good agreement. Several vertical lines indicate false positives/negatives or detection errors caused by noises. **b** BR averaged every two consecutive BRs detected by the PZT sensor system (BR-PZT: upper) and that by IPG (BR-IPG: lower), which were in good agreement.

val surrounded by several abnormal intervals (i.e., noisy condition) was scored as a failure to avoid overestimation. This automatic analysis method seems to be reliable because a HR detection rate of 95.7% during 10,000 s of representative data, including signal artifacts in part, was only 0.4% lower than that after a thorough manual correction. In ECG analysis, an HR between 100 and 200 beats/min was scored as correct. Finally, the HR detection rate, i.e., % time of successful cardiac cycle detection to total recording time, was calculated and compared between the PZT sensor and ECG measurements.

Similarly, the BR detection rate between the PZT sensor and IPG was compared by template search analysis and a spreadsheet application after band-pass filtering of 0.5–0.6 and 0.5–0.8 Hz, respectively. These comparisons were performed on selected data area with fewer motion artifacts, which were distinguished by analyzing template search analysis data; e.g., peak amplitude, maximum rise slope, instantaneous frequency, change in peak-peak interval and change in peak amplitude.

As the evaluations of false positive and negative in bradycardia and apnea are difficult in the case when ECG/IPG missed signals although the PZT signal was good, and because of huge data size, only false negatives in bradycardia/apnea detection were evaluated during the period when ECG/IPG detected bradycardia/apnea. Bradycardias of <80 beats/min for >5 s and apneas of >15 s in 27 and 11 neonates, respectively, were compared between the PZT sensor system and ECG/IPG.

Assessment of Discomfort

To assess whether the PZT sensor under the body is uncomfortable for a neonate, we compared the total amount of body movements of neonates with and without the PZT sensor. A cluster of body movements was counted when the baseline deflection of raw IPG signal exceeded ±2 V and it was repeated at intervals of <20 s, and the time between the first and last deflection was determined as the duration of body movement. The total time of body movements, including brief movements (twitch), was summed over the period of measurement in each neonate using a spreadsheet application. Ten newborn infants (5 boys and 5 girls; 2 VLBW and 8 LBW; median GA = 35.2 weeks; median BW = 2,029 g), with no complications were subjected to ECG measurement without the PZT sensor to compare with the data of 10 neonates (6 boys and 4 girls; 2 VLBW, 6 LBW and 2 normal weight; GA = 34.0 weeks; BW = 2,152 g) who underwent ECG with the PZT sensor recording (table 1). For the latter 10 neonates, 2/27 and 8/11 subjects were chosen from among the neonates who underwent the HR and BR (brief/long) assessment, respectively. No significant difference was found in GA ($p = 0.31$), weight ($p = 0.83$) and Apgar score ($p = 0.11$; 9 vs. 10, at 5 min, median) between the 2 groups with and without the PZT sensor recording.

Statistical Analysis

Statistical significance between groups was assessed depending on the homogeneity of variance by Student's t test or Welch's t test. Wilcoxon's non-parametric test was also applied to reveal significant differences. Data are expressed as the mean ± SD, and $p < 0.05$ was considered significant. Mann-Whitney's U test was used for the comparison of Apgar scores.

Results

We successfully detected heart sounds and breathing movements of newborn infants in the preliminary study using our custom-designed PZT sensor and an electric circuit similar to the cardiorespiratory monitor for mice (fig. 2) [7–9]. Differences in the signal waveform of heart

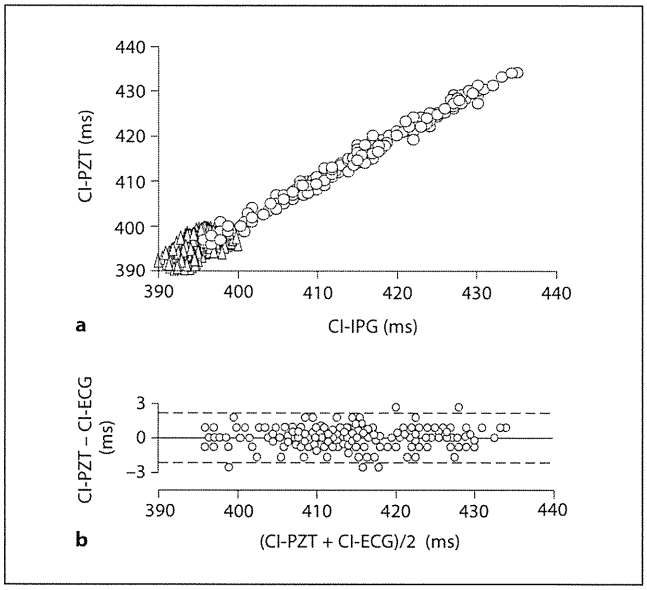

Fig. 4. Results of brief analysis of cardiac interval detection. Representative cross-correlation (**a**; open circles, r = 0.99) and difference plots (**b**) between the cardiac interval (CI) detected by PZT sensor (CI-PZT) and that by ECG (CI-ECG). Solid and broken lines indicate the means ± 2 SD. Superimposed open-triangle plots (**a**; r = 0.67) aggregated below the interval of 400 ms depict reduced heart rate variability of 1 ELBW patient.

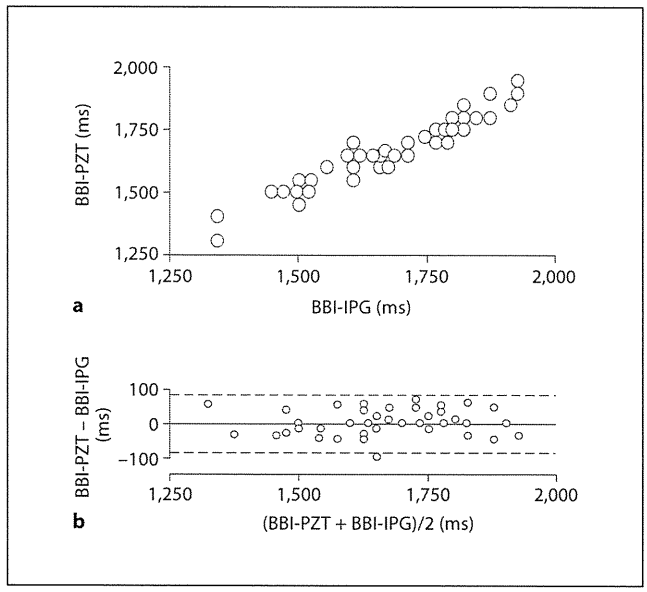

Fig. 5. Result in brief analysis of breathing interval detection. Representative cross-correlation (**a**; open circles, r = 0.96) and difference plots (**b**) between the breath-to-breath interval (BBI) detected by PZT sensor (BBI-PZT) and that by IPG (BBI-IPG). Solid and broken lines indicate the means ± 2 SD.

sounds and breathing movement between 4 sleeping positions (supine, prone, right or left side down) were not large enough to disturb template search analysis to detect cardiac and breathing intervals.

Brief analysis showed comparable performance of the PZT sensor for HR/BR detection to ECG/IPG when neonates were stable. Average cross-correlation coefficients and differences between the cardiac interval detected by the PZT sensor system and ECG were 0.92 ± 0.12 and −0.014 ± 0.035 ms (n = 27), respectively (table 2; fig. 4), and those between the breathing interval detected by the PZT sensor system and IPG were 0.95 ± 0.02 and −0.25 ± 1.45 ms (n = 11), respectively (table 3; fig. 5). Bland-Altman plots showed that 96.8 ± 2.0 and 95.2 ± 2.2% of plots of differences in cardiac and breathing intervals, respectively, fell within ±2 SD of their mean values (tables 2, 3; fig. 4b, 5b). In addition, cross-correlation plots of an ELBW patient markedly aggregated with small HR variation (fig. 4a; open triangles).

Long assessment of HR and BR detection by the PZT sensor was also successful when the body movement of a neonate was small and infrequent (fig. 3); however, the measurement was often disturbed by body movements, mechanical ventilation, routine care and breastfeeding by the mother, etc., some of which required the neonate to be held by the mother or nurses, and consequently ECG electrodes became dislodged. These interferences impaired heart sounds and breathing movement signals as well as ECG and IPG (fig. 6). The HR detection rate by the PZT sensor and ECG in all 27 neonates examined was 82.6 ± 12.9 and 91.8 ± 4.1% (p = 0.001), respectively, while comparable in ~70% (18/27; from top in table 2) of measurements (90.2 ± 4.1 vs. 92.0 ± 3.4%; p = 0.078, Student's paired t test; p = 0.054, Wilcoxon signed rank test).

Similarly, the BR detection rates in 11 neonates are summarized in table 3. The BR detection rates obtained by the PZT sensor system and IPG were 95.9 ± 4.0 and 95.3 ± 3.5%, respectively (p = 0.38, Student's paired t test; p = 0.15, Wilcoxon signed rank test), during the period with fewer motion artifacts and other extrinsic disturbances. % time of the period was 76.0 ± 12.5 and 77.1 ± 13.5% (p = 0.86, Student's paired t test) of the total time of PZT and IPG recording, respectively. Short periods of

Table 2. Long (1–9 days) period assessment of HR detection rate (total time of successful HR detection/total measurement time) in PZT sensor measurement (PZT) and ECG, and brief (1 min) assessment of correlation coefficient and difference of cardiac interval between the PZT sensor measurement and ECG

Patient No.	Sex	Long period assessment			Brief assessment				Body weight g
		HR detection rate		duration of measurement days	average HR beats/min	correlation coefficient r	difference ± SD ms	number of plots < ±2 SD, %	
		PZT, %	ECG, %						
1	M	97.1	88.7	3	124	0.981	−0.032 ± 2.72	98.4	2,222
2	F	95.5	96.9	7	132	0.892	−0.136 ± 3.89	94.7	1,272
3	M	94.6	92.6	7	125	0.986	−0.000 ± 1.73	93.7	1,555
4	F	94.2	93.0	7	143	0.993	0.007 ± 1.12	96.5	1,582
5	M	94.0	96.0	8	141	0.986	0.014 ± 1.18	100	1,287
6	M	94.0	86.3	1	125	0.979	−0.000 ± 1.67	96.8	2,182
7	M	93.6	91.3	7	165	0.828	−0.109 ± 2.63	98.8	1,252
8	F	91.6	96.1	7	111	0.983	−0.000 ± 2.99	97.7	1,835
9	M	90.4	94.2	7	149	0.984	0.013 ± 1.33	98.8	2,082
10	M	89.8	94.1	3	126	0.997	0.016 ± 1.74	96.9	2,392
11	M	87.7	91.9	5	132	0.999	−0.015 ± 1.55	97.0	2,617
12	F	87.5	92.0	3	129	0.906	−0.000 ± 1.38	97.7	4,126
13	F	86.9	89.8	3	146	0.834	0.014 ± 1.40	97.3	1,960
14	F	86.3	97.4	9	180	0.432	−0.011 ± 1.66	95.8	912
15	M	86.0	89.9	4	131	0.921	0.008 ± 1.15	100	2,307
16	M	86.0	96.6	7	157	0.947	−0.000 ± 1.21	96.1	2,140
17	M	85.5	92.7	4	116	0.970	−0.017 ± 2.44	91.7	1,555
18	F	83.9	86.1	3	142	0.955	0.000 ± 1.51	96.5	1,932
19	F	82.3	87.8	4	130	0.991	−0.023 ± 2.27	95.4	3,496
20	M	77.2	88.2	5	142	0.941	0.007 ± 1.01	97.3	1,422
21	M	72.6	97.5	1 (10 h)	115	0.992	−0.035 ± 2.96	98.3	2,718
22	M	71.1	86.2	3	148	0.929	−0.020 ± 1.37	95.3	3,437
23	M	68.5	85.4	5	133	0.987	−0.038 ± 2.06	98.5	2,516
24	M	66.5	88.2	6	145	0.973	−0.000 ± 1.13	96.6	2,288
25	M	62.1	97.1	7	165	0.666	−0.026 ± 1.65	94.0	742
26	M	57.0	86.4	7	140	0.992	−0.014 ± 1.84	94.4	1,856
27	M	47.9	96.5	8	166	0.914	0.013 ± 1.48	98.8	1,047

breathing cessation (apnea) and irregular breathing were comparably detected by the PZT sensor and IPG during long measurement (fig. 6a, left lower; 6b, right).

Bradycardias of <80 beats/min for >5 s (fig. 7) and apneas for >15 s (fig. 6a, left lower) were found in 6/27 and 5/11 neonates, respectively. False negatives in the bradycardias were 4% (4/44 in 5 of the 6 neonates; 1 deselected patient was ventilated with high frequency oscillation (HFO) and showed false negatives of 82% due to signal contamination; fig. 8), and among apneas false negatives were found in 1 case (6%; 1/17 in 5 neonates) due to weak signal intensity. In addition, total dislodging time of ECG electrodes in the 27 and 11 neonates during long measurement was 3,362 ± 1,893 s (0.8 ± 0.4%) and 3,547 ± 3,141 s (1.2 ± 0.8%), respectively.

Interference of the PZT sensor with neonates was not perceivable as the difference in % time of body movements between measurements by the PZT sensor with ECG (24.0 ± 12.5%) and those by ECG alone (22.9 ± 13.5%) was not significant (n = 10; p = 0.86, Student's unpaired t test; p = 0.92, Mann-Whitney U test; fig. 9). Although complications were diagnosed only in the PZT sensor group, the result may be not biased because the amounts of motility of 3 patients with complications were near the middle of the list (3rd, 6th and 7th). In addition, the fact that extrinsic artifacts due to treatment by physicians and nurses or parents may have been included in the motion artifacts was not considered in this analysis. In all 69 neonates who underwent the measurement with the PZT sensor, there was no skin damage with severity

Table 3. Long (1–4 days) period assessment of BR detection rate (total time of successful BR detection/total measurement time) in PZT sensor measurement (PZT) and impedance pneumography (IPG), and brief (1 min) assessment of correlation coefficient and difference of breathing interval between the PZT sensor measurement and IPG

Patient No.	Sex	Long period assessment					Brief assessment				Body weight g
		BR detection rate		non-move time		duration of measurement days	average BR beats/min	correlation coefficient r	difference (mean ± SD) ms	plots <±2SD %	
		PZT, %	IPG, %	PZT, %	IPG, %						
1	F	99.2	99.1	69.2	73.9	2	39	0.94	−0.26 ± 43	5.1	1,917
2	M	99.0	99	72.8	73.3	3	39	0.96	−1.28 ± 42	2.6	1,755
3	F	98.0	95.6	68.8	62.8	3	52	0.93	0.96 ± 45	3.8	2,232
4	M	98.0	96.3	75.1	65.4	4	58	0.93	0.00 ± 45	8.6	2,146
5	F	97.9	98.6	66.8	61.3	4	28	0.95	3.93 ± 70	3.6	1,236
6	F	97.8	97.3	71.1	76.2	4	82	0.93	0.13 ± 27	1.2	2,852
7	M	96.5	95.6	75.5	77.8	3	67	0.92	0.90 ± 40	4.5	2,288
8	M	95.9	95.3	76.9	81.4	1	56	0.98	−0.89 ± 32	7.1	2,157
9	F	94.0	93.7	72.9	77.7	4	61	0.99	−0.56 ± 9	4.8	2,630
10	M	92.9	89	70.8	67.0	4	46	0.98	−0.43 ± 45	6.5	1,117
11	F	85.3	89.1	70.6	75.6	4	45	0.94	0.21 ± 30	4.4	3,316

Non-move time = Total time of periods with no large signal perturbation during measurement.

of stages I, II and III, from slight erythema to an abrasion [1], at sides (right/left), back or chest/abdomen. Moreover, the PZT sensor did not disturb the arrangement of other tubes or catheters attached to the neonate or the routine work of physicians and nurses.

Discussion

Cardiorespiratory monitoring by the proposed PZT sensor is likely to be highly noninvasive for neonates, as the PZT sensor caused no skin damage and did not increase body movement (fig. 9) as an index of discomfort [10–12]. Physicians who performed PZT sensor measurement did not perceive any difference in the attitude of neonates with and without the PZT sensor, although a small stress due to the PZT sensor may have been masked by the many tubes, catheters and adhesive plasters attached to a neonate. Accordingly, the thin-shaped PZT sensor with several holes, which never comes into contact with the neonate's skin, may be suitable for keeping a neonate comfortable during long-term cardiorespiratory monitoring in an incubator (fig. 1).

Brief assessment of HR and BR detection showed that the PZT sensor has an inherently high performance comparable to ECG and IPG (r = 0.92 and 0.95), consistent with a previous study in mice [7]. In addition, aggregated plots of the HR of an ELBW patient (fig. 4a; open triangles) suggest that the PZT sensor can also be used to analyze HR variability, which has been considered to be a prognostic risk indicator of life-threatening diseases including sudden infant death syndrome (SIDS).

Long assessment of PZT sensor measurements again showed a high HR detection rate (~90%) comparable to ECG in a large part (18/27) of the measurements (table 2). While, a small group (5/27) showed a lower HR detection rate of <70% (68.5–47.9%), although it was not continuously low throughout the measurement, but it was >80% for 1–2 days in 3 of 5 neonates. The lower HR detection rate was due to HFO ventilation in 2 neonates, frequent body movements in 1 neonate and weak signal intensity in another one (being transferred from a closed incubator to an open cot may have been the cause in 1 neonate). In addition, frequent changes of sleeping position among neonates might have influenced the HR detection rate. Since these lower HR detection rates might have been higher if the PZT signal had been displayed continuously on a monitor screen and sufficient attention to the sensor settings had been paid by physicians or nurses, and since the false-negative value in bradycardia detection was low (4%), the capacity of the PZT sensor for long HR measurement is probably sufficient for practical use in the NICU.

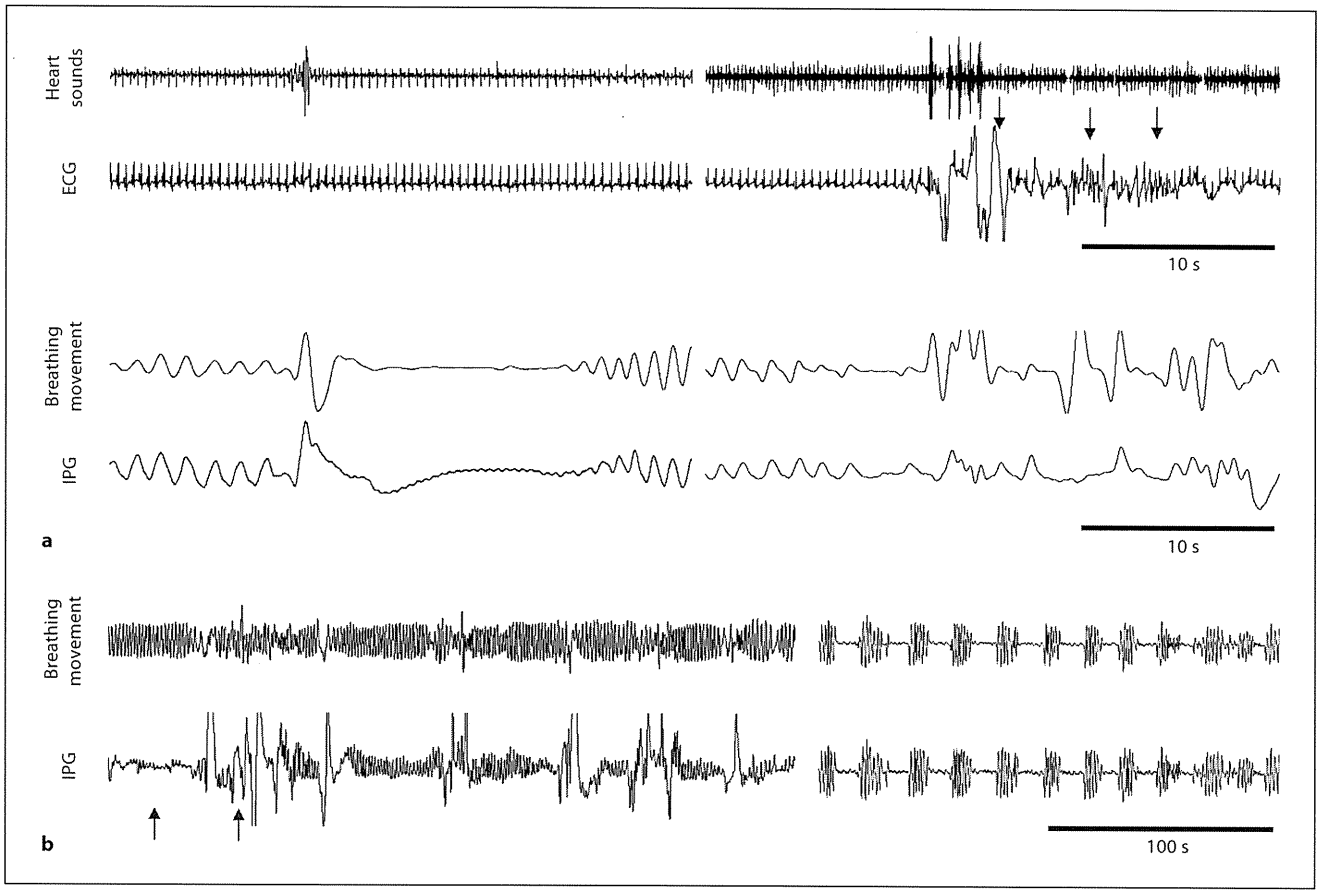

Fig. 6. Signal perturbations appeared during the simultaneous measurement of PZT sensor system and ECG/IPG. **a** From top to bottom: heart sounds obtained by the PZT system, ECG, breathing movement obtained by the PZT system and impedance pneumography (IPG). Each 4 signals in the left and right half-panels were recorded simultaneously. Left panel shows signal perturbations in heart sounds and ECG induced by a brief cessation (~15 s) of breathing (apnea; lower 2 traces). Right panel shows signal perturbations induced by a large body movement. S_1 signal is dominant in the heart sounds in the left panel, while S_1 and S_2 in the right panel are comparable. Several R waves in ECG are inarticulate compared to the S_1 and S_2 (arrows) during the body movement. **b** Signal perturbation in IPG signal was often larger than in PZT sensor signal, i.e., breathing movement (left). Breathing signal was often inarticulate in IPG (arrows) in contrast to PZT sensor signal. Irregular breathing pattern was similarly detected by both methods (right).

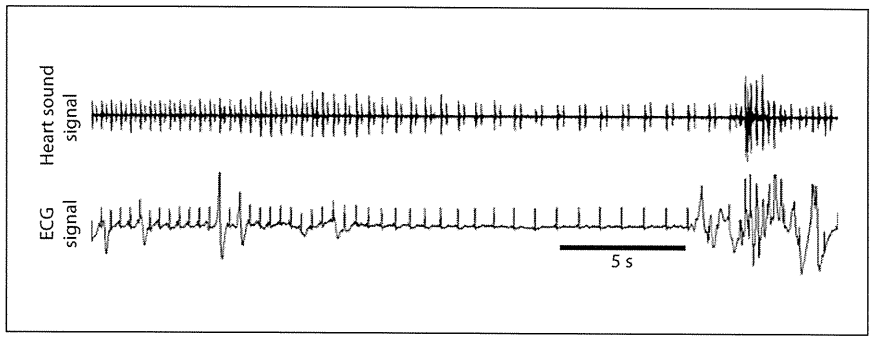

Fig. 7. Representative traces of bradycardia recorded by the PZT sensor system (upper) and ECG (lower). Heart sounds and R waves were clearly detected, and both cardiac intervals were gradually increased until a body movement emerged.

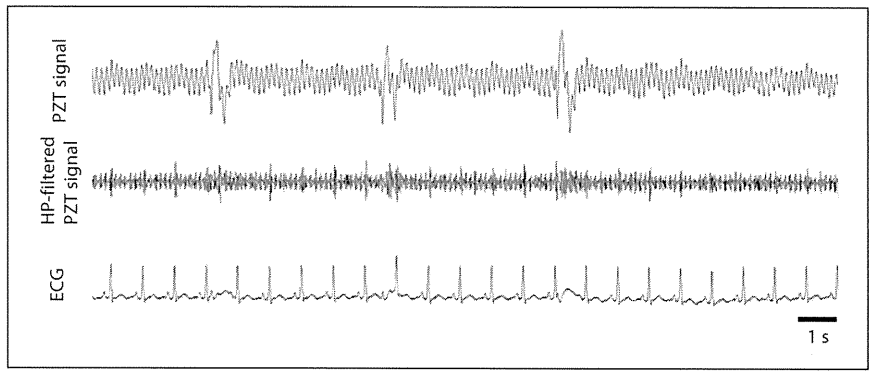

Fig. 8. PZT sensor output signal (PZT signal) influenced by mechanical ventilation (high frequency oscillation, HFO). The signal is severely contaminated with artifact of HFO (upper trace). High-pass (HP) filtering reduced the noise and several S_1 peaks are distinguishable by human eyes (middle trace), which corresponded to R waves in ECG (lower trace), but not by automatic template search analysis.

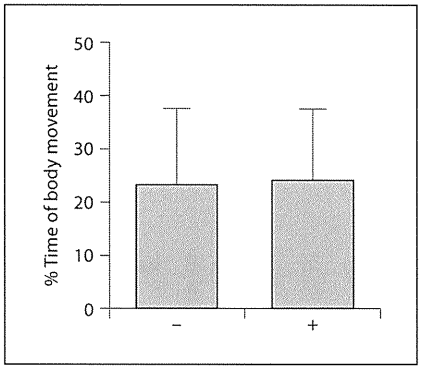

Fig. 9. Effect of PZT sensor placement on body movements of neonates. There was no significant difference in the mean (±SD) %time of body movement between neonates with (+) and without (–) the PZT sensor (n = 10, p = 0.86, Student's unpaired t test).

Cardiac monitoring by the PZT sensor provides us additional information on a lower frequency range, complimenting information obtained by a conventional stethoscope, which was developed by Laennec in 1819 [13]. The lower frequency signal that probably represents gross heart movement (fig. 2; arrows) may have useful information for clinical diagnoses [Sato et al., unpublished data] in addition to heart murmurs and accentuated second sounds [14–16]. Visualized heart and lung sound signals may contribute to increasing the detection rate of cardiac function anomalies, excluding innocent heart murmurs [15–19]. It may also be possible to predict an adverse neurologic outcome at 1 year of age by analyzing abnormal general movements [20–23], which can be detected by the PZT sensor.

It was reported that respiratory activity monitoring by a similar PZT sensor was in good agreement with that by a CO_2 respiratory monitor [24] or a thermistor airflow sensor [7] in mice. However, a large deformation of respiratory signal due to motion artifacts, routine care and artificial ventilation made BR evaluation impossible in about 30% of the total recording time in the present study (table 3). Respiratory-signal deformation is also a recognized problem in IPG [25–29] (fig. 6a, right; 6b, left lower). As a consequence, the BR detection rate was compared between the PZT sensor and IPG using ~70% of total data, which resulted in considerably good agreement (fig. 5; table 3). As the impairment of respiratory signals often occurred either in the PZT signal or IPG but not always at the same time (fig. 6b, left lower, arrows), respiratory monitoring with both a PZT sensor and IPG might reduce the false alarms that often disturb nurses in the NICU. In addition, as both methods detect different information on respiratory activity from different sites on a neonate's body, it might be of help in discriminating between central sleep apnea and obstructive sleep apnea [Sato et al., unpublished data], and also in studying sudden infant death syndrome [30].

In the present study, long-term assessment was limited by compromised evaluation due to the huge data size. Nonetheless, according to the comparable HR detection rate (difference 0.4%) in a representative 10,000 s data between automatic analysis with and without a thorough manual verification, we believe that errors in HR/BR detection rate with the simplified manual verification were mostly within ± 1%. A more practical assessment will be performed after manufacturing a real-time PZT sensor-based cardiorespiratory monitor for newborns in the NICU.

Many types of other PZT sensors for cardiorespiratory monitoring have been proposed. They are generally susceptible to motion and have disadvantages for use in the

NICU; for example, a mattress-type sensor seems to be difficult to handle in an incubator, to sterilize and let babies sleep comfortably. In contrast, our PZT sensor was made as small as possible to impede motion artifacts from a wider area, and a form mattress under the PZT sensor attenuates extrinsic vibration from the floor propagating through the bed frame of an incubator, although the artifact of HFO is still unavoidable. The influence of the HFO on heart sound signal should be resolved by advanced signal-processing algorithms such as pattern recognition, wavelet transforming or independent component analysis [17, 31, 32] since the human eye can distinguish S_1 from HFO noise (fig. 8, middle trace). The PZT sensor also showed strong durability for repetitive use of over 12 months; it is easy to handle, to sterilize and to use over a long duration without changing the sensor because it causes no skin irritation and because one does not have to worry about wet-gel drying up that deteriorates signal quality when using ECG electrodes.

In addition, we often observed a loss of ECG/IPG signal for several to 10 s of minutes although the PZT sensor signal recorded continuously, which suggests that the two systems can help each other when either one fails to detect a signal. Accordingly, the PZT sensor system can be used as a backup cardiorespiratory monitor for a more secure monitor system, or as a main cardiorespiratory monitor for a healthier infant who does not necessarily require full ECG information. Furthermore, the system may serve well as an advanced diagnostic tool for cardiac diseases because it utilizes the PZT system and analyzes information derived from both acoustic cardiography and ECG [15, 16, 18].

In conclusion, the PZT sensor is noninvasive and does not cause skin irritation, but we believe it does provide reliable, accurate measurements for monitoring of long-term cardiorespiratory activity of neonates in the NICU, although the issue of mechanical ventilation noise (HFO in particular) remains to be solved.

Acknowledgements

This work was supported in part by the Vehicle Racing Commemorative Foundation, Unique Medical Co., Ltd., Fukuda Denshi Co., Ltd., AT Labo Co., Ltd. and an intramural grant from Akita University School of Medicine. The authors thank the staff of the NICU at Akita University Hospital, and Kumi Sato and Qing Liu for their technical contributions to data analysis.

References

1 Barak M, Hershkowitz S, Rod R, Dror S: The use of a synthetic skin covering as a protective layer in the daily care of low birth weight infants. Eur J Pediatr 1989;148:665–666.

2 Di Rienzo M, Rizzo F, Meriggi P, Bordoni B, Brambilla G, Ferratini M, Castiglioni P: Applications of a textile-based wearable system for vital signs monitoring. Conf Proc IEEE Eng Med Biol Soc 2006;1:2223–2226.

3 Brouillette RT, Morrow AS, Weese-Mayer DE, Hunt CE: Comparison of respiratory inductive plethysmography and thoracic impedance for apnea monitoring. J Pediatr 1987;111:377–383.

4 DeGroff CG, Bhatikar S, Hertzberg J, Shandas R, Valdes-Cruz L, Mahajan RL: Artificial neural network-based method of screening heart murmurs in children. Circulation 2001;103:2711–2716.

5 Kleinman CS: Cardiac ultrasonography in the fetus and newborn. Mead Johnson Symp Perinat Dev Med 1987;25:32–39.

6 Ommen SR, Nishimura RA, Appleton CP, Miller FA, Oh JK, Redfield MM, Tajik AJ: Clinical utility of Doppler echocardiography and tissue Doppler imaging in the estimation of left ventricular filling pressures: a comparative simultaneous Doppler-catheterization study. Circulation 2000;102:1788–1794.

7 Sato S, Yamada K, Inagaki N: System for simultaneously monitoring heart and breathing rate in mice using a piezoelectric transducer. Med Biol Eng Comput 2006;44:353–362.

8 Sato S: Cardiac beat detector – a novel analogue circuitry for the first heart sound discrimination. Biosignals Proc 2008;2:136–140.

9 Sato S: Quantitative evaluation of ontogenetic change in heart rate and its autonomic regulation in newborn mice with the use of a noninvasive piezoelectric sensor. Am J Physiol Heart Circ Physiol 2008;294:H1708–H1715.

10 Ratcliffe JM: Sedation in the intensive care unit. Curr Pediatr 1994;4:106–109.

11 Playfor SD, Thomas DA, Choonara I, Collier J, Jarvis A: Parental perceptions of comfort during mechanical ventilation. Paediatr Anaesth 2001;11:99–103.

12 Hadjistavropoulos HD, Craig KD, Grunau RE, Whitfield MF: Judging pain in infants: behavioural, contextual, and developmental determinants. Pain 1997;73:319–324.

13 Noonan JA: A history of pediatric specialties: the development of pediatric cardiology. Pediatr Res 2004;56:298–306.

14 Levi DS, Kusnezov N, Carman GP: Smart materials applications for pediatric cardiovascular devices. Pediatr Res 2008;63:552–558.

15 Larkin M: Paediatric heart sounds assessed by computer. Lancet 2001;357:1856.

16 Erne P: Beyond auscultation – acoustic cardiography in the diagnosis and assessment of cardiac disease. Swiss Med Wkly 2008;138:439–452.

17 Debbal SM, Bereksi-Reguig F: Computerized heart sounds analysis. Comput Biol Med 2008;38:263–280.

18 Noponen AL, Lukkarinen S, Angerla A, Sepponen R: Phono-spectrographic analysis of heart murmur in children. BMC Pediatr 2007;7:23.

19 Smith KM: The innocent heart murmur in children. J Pediatr Health Care 1997;11:207–214.

20 Lüchinger AB, Hadders-Algra M, van Kan CM, de Vries JI: Fetal onset of general movements. Pediatr Res 2008;63:191–195.

21 Hadders-Algra M, Mavinkurve-Groothuis AM, Groen SE, Stremmelaar EF, Martijn A, Butcher PR: Quality of general movements and the development of minor neurological dysfunction at toddler and school age. Clin Rehabil 2004;18:287–299.

22 Prechtl HF, Einspieler C, Cioni G, Bos AF, Ferrari F, Sontheimer D: An early marker for neurological deficits after perinatal brain lesions. Lancet 1997;349:1361–1363.
23 Groen SE, de Blecourt AC, Postema K, Hadders-Algra M: General movements in early infancy predict neuromotor development at 9 to 12 years of age. Dev Med Child Neurol 2005;47:731–738.
24 Miyake A, Yamada K, Kosaka T, Miki T, Seino S, Inagaki N: Disruption of Kir6.2-containing ATP-sensitive potassium channels impairs maintenance of hypoxic gasping in mice. Eur J Neurosci 2007;25:2349–2363.
25 Khambete ND, Brown BH, Smallwood RH: Movement artefact rejection in impedance pneumography using six strategically placed electrodes. Physiol Meas 2000;21:79–88.
26 Ernst JM, Litvack DA, Lozano DL, Cacioppo JT, Berntson GG: Impedance pneumography: noise as signal in impedance cardiography. Psychophysiology 1999;36:333–338.
27 Cohen KP, Ladd WM, Beams DM, Sheers WS, Radwin RG, Tompkins WJ, Webster JG: Comparison of impedance and inductance ventilation sensors on adults during breathing, motion, and simulated airway obstruction. IEEE Trans Biomed Eng 1997;44:555–566.
28 Rosell J, Webster JG: Signal-to-motion artifact ratio versus frequency for impedance pneumography. IEEE Trans Biomed Eng 1995;42:321–323.
29 Adams JA, Zabaleta IA, Stroh D, Sackner MA: Measurement of breath amplitudes: comparison of three noninvasive respiratory monitors to integrated pneumotachograph. Pediatr Pulmonol 1993;16:254–258.
30 Ramanathan R, Corwin MJ, Hunt CE, Lister G, Tinsley LR, Baird T, Silvestri JM, Crowell DH, Hufford D, Martin RJ, Neuman MR, Weese-Mayer DE, Cupples LA, Peucker M, Willinger M, Keens TG: Cardiorespiratory events recorded on home monitors. JAMA 2001;285:2199–2207.
31 Nazeran H: Wavelet-based segmentation and feature extraction of heart sounds for intelligent PDA-based phonocardiography. Methods Inf Med 2007;46:135–141.
32 Matsumoto M, Hashimoto S: An acoustical array combining microphones and piezoelectric devices. J Acoust Soc Am 2008;123:2117–2125.

JAPANESE DERMATOLOGICAL ASSOCIATION
THE JOURNAL OF DERMATOLOGY

doi: 10.1111/j.1346-8138.2010.00932.x

Journal of Dermatology 2010; **37**: 956–964

ORIGINAL ARTICLE

Expression of wild-type, but not mutant, loricrin causes programmed cell death in HaCaT keratinocytes

Kozo YONEDA,[1] Toshio DEMITSU,[2] Motomu MANABE,[3] Junsuke IGARASHI,[4] Hiroaki KOSAKA,[4] Nobuya INAGAKI,[5] Hidetoshi TAKAHASHI,[6] Atsushi KON,[7] Maki KAKURAI,[2] Yasuo KUBOTA[1]

[1]*Department of Dermatology, Faculty of Medicine, Kagawa University, Kagawa,* [2]*Department of Dermatology, Jichi Medical University Omiya Medical Center, Saitama,* [3]*Department of Dermatology, Akita University School of Medicine, Akita,* [4]*Cardiovascular Physiology, Faculty of Medicine, Kagawa University, Kagawa,* [5]*Department of Diabetes and Clinical Nutrition, Kyoto University Graduate School of Medicine, Kyoto,* [6]*Department of Dermatology, Asahikawa Medical College, Hokkaido, and* [7]*Department of Biochemistry, Hirosaki University School of Medicine, Hirosaki, Japan*

ABSTRACT

The epidermal cornified cell envelope is a complex protein–lipid composite that replaces the plasma membrane of corneocytes and is crucial for epidermal barrier function. Loricrin is a major constituent of the epidermal cornified cell envelope, contributing approximately 70% by mass. In order to explore novel function of wild-type (WT) loricrin other than the major component of the epidermal cornified cell envelope, we transiently expressed construct encoding human WT and mutant loricrin (730insG) in HaCaT keratinocytes. HaCaT cells transfected with WT or mutant loricrin were at differentiation level. WT loricrin in the transfected cells was seen diffusely in the cytoplasm and nuclei. Positive transferase deoxytidyl uridine end labeling staining was observed in the nuclei of WT loricrin-transfected HaCaT keratinocytes. Data from the DNA fragmentation assay showed that only WT loricrin induced DNA ladders compared with that of mutant loricrin. WT loricrin-transfected HaCaT keratinocytes were susceptible to programmed cell death (PCD). Activation of caspase-14 was also seen. In contrast, PCD or activation of caspase-14 did not occur in mutant loricrin-transfected HaCaT cells. These results suggest that the expression of WT loricrin facilitates induction of PCD in HaCaT keratinocytes.

Key words: caspase-14, cornified cell envelope, loricrin, programmed cell death.

INTRODUCTION

Loricrin is a glycine-, serine- and cystein-rich basic protein expressed in the granular cell layer of the epidermis, where it is first stored in aggregates (L-granules in mouse, keratohyalin granules in human) that are predominantly cytoplasmic, but also seen in the nucleus.[1–6] In the last stage of terminal differentiation, these aggregates are dispersed and loricrin is assembled into the cornified cell envelope where it is cross-linked with the other cornified cell envelope components. Recently, mutations in the loricrin gene have been reported in Vohwinkel syndrome with ichthyosis (Online Mendelian Inheritance in Man [OMIM] 604117).[7–17] Furthermore, Ishida-Yamamoto *et al.*[14] identified a similar loricrin mutation in a family with progressive symmetric erythrokeratoderma (OMIM 602036). These syndromes are now collectively named loricrin keratoderma. So far, four types of loricrin mutations have been detected in genomic DNA from nine families. The most frequent mutation, 730insG, has been found in families from the UK, Japan and Germany. A defective protein generated from the mutant loricrin allele in Vohwinkel syndrome

Correspondence: Kozo Yoneda, M.D., Ph.D., Department of Dermatology, Faculty of Medicine, Kagawa University, Kagawa 761-0793, Japan.
Email: kyoneda@med.kagawa-u.ac.jp
Received 9 February 2010; accepted 28 March 2010.

is unusual. It generates a frame-shift before its terminal 84 codons, which further extends the polypeptide 22 amino acids beyond the C-terminal domain of the wild-type (WT) protein. This C-terminal domain of the mutant, but not WT, loricrin polypeptide is predicted to contain a nuclear localization signal. To explore the molecular mechanisms for abnormal keratinization caused by mutant loricrin, it is essential to know the function of WT and mutant loricrin *in vivo* and *in vitro*.

In this study, we sought to determine the function of WT loricrin in HaCaT keratinocytes using transient transfection as a means of ectopic protein expression. We report here that expression of human WT, but not mutant, loricrin leads to programmed cell death (PCD) with the activation of caspase-14.

METHODS

Plasmid construction

Genomic DNA containing the entire coding region of WT loricrin[1] and mutant loricrin[10] was subcloned into pcDNA 3.1/V5-His vector (Invitrogen, San Diego, CA, USA). The most frequent mutation, 730insG, was chosen for the present study. The sequence of each of the plasmid constructs was verified by the dideoxynucleotide chain termination method using the 377 DNA sequencing system (Applied Biosystems, Foster City, CA, USA).

Cell culture and plasmid transfection

The culture and transfection of HaCaT cells were carried out as previously described.[18,19] Briefly, cells were plated on 35 or 60 mm culture dishes at a density of 4×10^5 cells/mL 24 h before plasmid transfection, and cultured in Dulbecco's modified Eagle's medium (450 mg/dL glucose) supplemented with 10% (v/v) fetal bovine serum. A portion of 2 μg of WT loricrin or mutant loricrin in pcDNA3.1/V5-His vector for 35-mm dishes and 10 μg for 100-mm dishes was transfected into cells with LipofectAMINE plus reagent (Invitrogen) according to the manufacturer's instructions. Forty-eight hours after transfection, cells were collected for further analysis. In each experiment, transfection efficiency was confirmed to be similar among types of transfected plasmids using X-gal staining. The percentage of cell death induced by WT loricrin was determined by transfecting cells with pcDNA3.1/V5-His vector (mock), pcDNA3.1/V5-His WT loricrin and pcDNA3.1/V5-His mutant loricrin. PCD cells were identified by visual inspection with a Nikon inverted fluorescence microscope (Nikon, Tokyo, Japan). The uptake of Trypan blue and SYTO 13 (Invitrogen) was used to confirm the number of PCD. Each experiment was performed at least five times, with 10 000 cells counted for each determination.

Primary antibodies

The anti-V5 antibody was purchased from Invitrogen, polyclonal rabbit anti-human keratin antibody from DAKO (Glostrup, Denmark), anti-caspase-14, anti-filaggrin, anti-transglutaminase-1, anti-involucrin and anti-α-tubulin antibody from Santa Cruz Biotech (Santa Cruz, CA, USA), and anti-envoplakin and anti-periplakin antibody from Abcam (Cambridge, UK).

Immunofluorescence microscopy

Immunostaining was performed exactly as described previously.[20] After 48 h of transfection, HaCaT cells on glass coverslips were fixed with methanol. Cells on glass coverslips were incubated with primary antibodies (anti-V5 [1:300], anti-keratin [1:200], anti-envoplakin [1:300], anti-periplakin [1:300], anti-involucrin [1:300], anti-transglutaminase-1 [1:300], and anti-filaggrin [1:300]) overnight at 4°C, and detection was made with fluorescein isothiocyanate-conjugated antibody to rabbit immunoglobulin (Ig)G or a combination of Cy3-conjugated streptavidin and biotin-conjugated antimouse IgG. Immunofluorescent images were viewed with a confocal laser microscope (Olympus, Tokyo, Japan).

Immunoblot analysis

Immunoblot analysis was performed exactly as described previously.[18] After 48 h of transfection, HaCaT cells were lysed in Laemli buffer (consisting of 62.5 mmol/L Tris-HCl (pH 6.8), 25% glycerol, 2% sodium dodecylsulfate [SDS], 0.01% bromphenol blue) on ice for 30 min. Cell debris was removed by centrifugation at 20 380 *g* for 1 min, and supernatant (cell lysates) was collected. Protein concentrations in cell lysates were determined using Bradford reagent (BioRad, Hercules, CA, USA). Cell lysates containing 30 μg proteins were electrophoresed on an SDS/polyacrylamide gel and transferred to a nitrocellulose membrane. The membrane was incubated with

primary antibody (anti-V5 [1:1000], anti-caspase-14 [1:5000] and anti-α-tubulin [1:200] antibody) for 2 h at room temperature, followed by incubation with horseradish peroxidase (HRP)-conjugated appropriate secondary antibody, and the proteins were detected using an enhanced chemiluminescence system (Amersham Biosciences, Piscataway, NJ, USA) according to the manufacturer's instructions.

TUNEL staining

Transferase deoxytidyl uridine end labeling (TUNEL) staining was performed with ApopTag apoptosis detection kit (Intergen, Burlington, MA, USA) exactly as described previously.[18] HaCaT cells on coverslips were fixed with −20°C methanol, rinsed with phosphate buffered saline (PBS) two times, and treated with 10% normal goat serum for 10 min. They were then incubated with the anti-V5 antibody for 30 min, rinsed with PBS three times, and incubated with biotin-conjugated goat antimouse IgG (Sigma, St Louis, MO, USA) for 30 min, followed by incubation with streptavidin–Cy3 conjugate (Sigma) for 30 min. Cells were incubated with working strength TdT enzyme at 37°C for 1 h, extensively washed with stop/wash buffer and PBS, and incubated with anti-digoxigenin conjugate fluorescent dye for 30 min. They were mounted on a glass slide with PermaFluor (Thermo-Shandon, Vernon Hills, IL, USA) and observed by confocal laser microscope (Olympus).

DNA fragmentation assay

After 48 h of transfection, HaCaT cells were lysed in lysis buffer (10 mmol/L Tris-HCl (pH 8.0), 100 mmol/L NaCl, 1% SDS, 1 mmol/L ethylene diamine tetra acetate, and 2 mg/mL proteinase K) for 1 h at 65°C. Following two successive extractions with phenol/chloroform, the DNA samples were precipitated in ethanol. After washing with 70% ethanol, the DNA samples were resuspended in TE buffer and subjected to 2% agarose gel electrophoresis.

Statistics

All values are presented as means ± standard error of the mean. The significance of the difference from the respective controls for each experiment test condition was assayed using a Student's *t*-test for each paired experiment. An ANOVA was used to test for significance ($P < 0.05$).

RESULTS

Subcellular localization of WT and mutant loricrin

Genomic DNA containing the coding region of WT loricrin and mutant loricrin was subcloned into pcDNA3.1/V5-His vector. The most frequent mutation, 730insG, was chosen for this study. The transfection efficiencies for WT and mutant loricrin were almost the same. Immunoblot analysis using anti-V5 antibody revealed that WT loricrin (Fig. 1a, arrow, 35 kDa) and mutant loricrin (arrowhead, 42 kDa) were expressed to almost the same degree (Fig. 1a). Although the expected molecular mass of WT loricrin is 35 kDa, the migrating position of WT loricrin was around the 37-kDa molecular marker. We think this migration is due to many aliphatic amino acids (glycine/serine/cystein) in WT loricrin. Next, to determine whether mutant loricrin protein localizes in the nucleus in cultured keratinocytes as in keratinocytes of loricrin keratoderma *in vivo*,[7] we transfected HaCaT cells with V5-tagged WT loricrin or mutant loricrin, the mutation in loricrin keratoderma, and stained them with an anti-V5 antibody and an anti-keratin antibody. WT loricrin distributes in the cytoplasm and nucleus (Fig. 1b, upper right panel). Mutant loricrin, which is predicted to get a nuclear localization signal, seems to localize in the nucleolus (Fig. 1c, upper right panel). Why it localizes in the nucleolus, rather than nucleus, is not clear as reported by Ishida-Yamamoto *et al.*[21] We analyzed 4 000 000 cells and found that transfection efficiency was the same in either semi-confluent or non-confluent state. That is, transfection efficiency was not dependent on confluency. When WT loricrin was transfected, we observed cells shrinking perhaps due to PCD.

Differentiation level of the HaCaT cells transfected with WT or mutant loricrin

At first, we transfected WT loricrin and mutant loricrin into normal human epidermal keratinocytes. Normal human epidermal keratinocytes were purchased from KURABO (Osaka, Japan). These primary human epidermal keratinocytes were cultured and transfected as described by DiColandrea *et al.*[22] However, we could not transfect WT and mutant loricrin constructs into normal human epidermal keratinocytes. That was

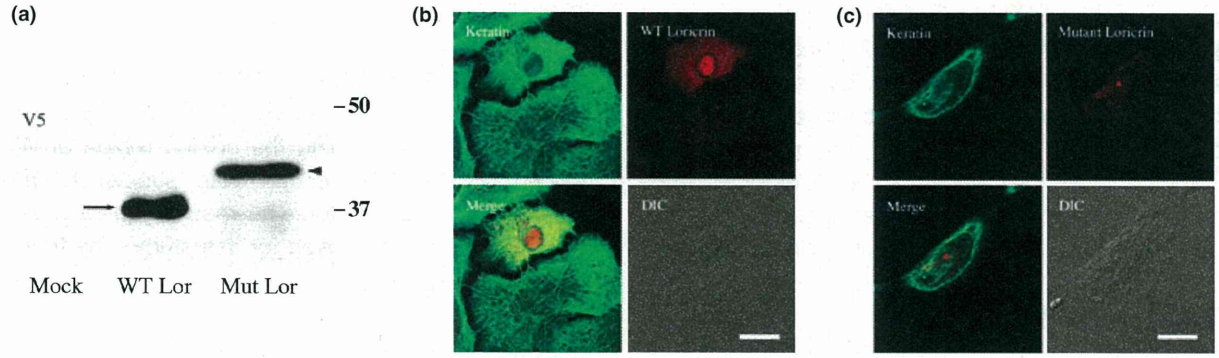

Figure 1. (a) Immunoblot analysis of wild-type (WT) loricrin-transfected HaCaT cells and mutant loricrn-transfected HaCaT cells. Immunoblot with anti-V5 antibody revealed that WT loricrin and mutant loricrin were expressed to almost the same degree. Arrow denotes 35-kDa WT loricrin including V5 tag sequence. Arrowhead denotes 42-kDa mutant loricrin including V5 tag sequence. Although the expected molecular mass of WT loricrin is 35 kDa, the migrating position of WT loricrin was around the 37-kDa molecular marker. We think this migration is due to many aliphatic amino acids (glycine/serine/cystein) in WT loricrin. (b,c) Distribution of WT loricrin-V5 and mutant loricrin-V5 of transfected HaCaT keratinocytes. HaCaT keratinocytes were transfected with either plasmid pcDNA3.1/V5-His-WT loricrin or plasmid pcDNA3.1/V5-His-mutant loricrin. Cells were fixed at 48 h post-transfection, and the fate of the transfected gene product was examined by double-label immunofluorescence. To visualize the transfected gene product, cells were stained with a mouse monoclonal antibody recognizing the sequence of V5. Antibody staining was followed by biotin-conjugated antimouse immunoglobulin G and Cy3-conjugated streptavidin. (b) Double-stainings of HaCaT cells with 1:100-diluted anti-V5 antibody (red) and 1:100-diluted anti-keratin antibody (green). WT loricrin distributes diffusely in the cytoplasm and in the nuclei in transfected cells. (Scale bars: 25 μm.) (c) Double-stainings of HaCaT cells with 1:100-diluted anti-V5 antibody (red) and 1:100-diluted anti-keratin antibody (green). Mutant loricrin distributes in the nucleolus as a V5-positive immunoreactive granule. (Scale bars: 25 μm.) DIC, differential interference contrast.

to say, transfection efficiency was so low (<0.1%) that we could not detect WT or mutant loricrin with immunoblot analysis. Then, we decided to use HaCaT cells. The HaCaT keratinocyte cell line is a spontaneously transformed human epithelial cell line derived from adult skin which maintains full epidermal differentiation capacity.[23] The transfection efficiency into HaCaT cells was approximately 3%. Because the expression of WT and mutant loricrin is observed only in morphologically different keratinocytes, we tried to estimate the differentiation level of WT and mutant loricrin transfected HaCaT cells. WT loricrin-transfected HaCaT cells exhibited positive immunoreactivities for periplakin, envoplakin, involucrin, transglutaminase 1 and filaggrin. Mutant loricrin-transfected HaCaT cells also exhibited positive immunoreactivities for periplakin, envoplakin, involucrin, transglutaminase 1 and filaggrin. Mutant loricrin in the nucleoli co-localized with periplakin, envoplakin, involucrin, transglutaminase 1 and filaggrin (Fig. 2). We could not transfect WT or mutant loricrin into non-differentiated level HaCaT cells (filaggrin-negative HaCaT cells). These results suggest that HaCaT cells expressing WT or mutant loricrin are at differentiation level because periplakin, envoplakin, involucrin, transglutaminase 1 and filaggrin are differentiation markers.

PCD and activation of caspases-14 in HaCaT cells expressing WT loricrin

To explore whether WT loricrin induces PCD in HaCaT cells, we first examined the effects of WT loricrin on cell morphology. Forty-eight hours after transfection, the number of cell deaths was determined by counting 10 000 HaCaT cells under a phase-contrast microsocpe. PCD cells were judged by staining both PCD nuclei with SYTO 13 and plasma-membrane permeabilization with Trypan blue. When WT loricrin was transfected, PCD cells which contained PCD nuclei were increased (Fig. 3a). PCD cells in 10 000 cells increased from 9 ± 2.2 of mock to 103 ± 4.3 of WT loricrin. In contrast, mutant loricrin did not increase PCD cells (8 ± 4.1 cells).

Furthermore, positive TUNEL stainings were observed in the nuclei in WT loricrin-transfected cells (Fig. 3b). Data from the DNA fragmentation assay showed that only WT loricrin induced DNA ladders

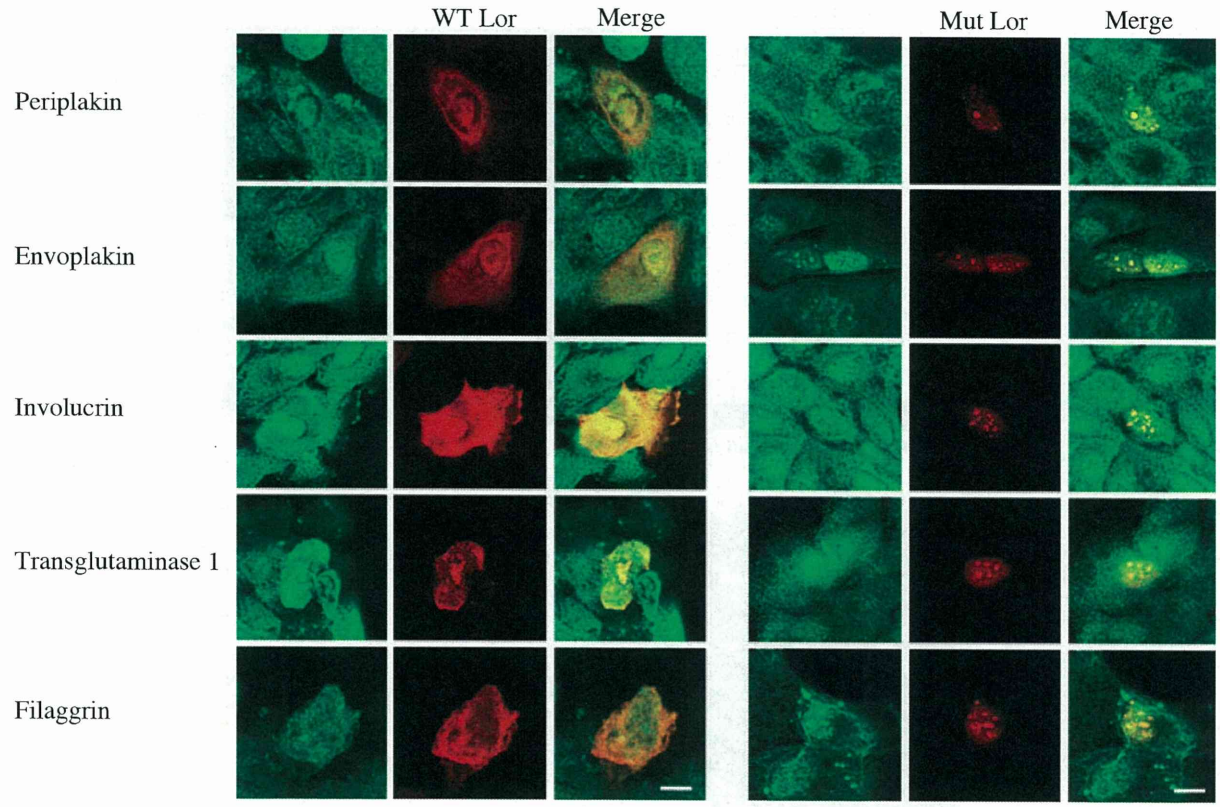

Figure 2. Differentiation level of the HaCaT cells after transfection of wild-type (WT) and mutant loricrin. WT loricrin-transfected HaCaT cells exhibited positive immunoreactivities for periplakin, envoplakin, involucrin, transglutaminase 1 and filaggrin. Mutant loricrin-transfected HaCaT cell also exhibited positive immunoreactivities for periplakin, envoplakin, involucrin, transglutaminase 1 and filaggrin. We could not transfect WT or mutant loricrin into non-differentiated level HaCaT cells (filaggrin-negative HaCaT cells). (Scale bars: 25 μm.)

(Fig. 3c). Immunoblot analysis using anti-caspase-14 antibody revealed that processing the p11 fragment was observed only in WT loricrin-transfected cells (Fig. 3d, arrow). Caspase-14 was not activated in mock or mutant loricrin-transfected HaCaT cells.

DISCUSSION

As far as we know, we showed for the first time that procaspase-14 was processed and activated accompanying PCD when we transfected WT loricrin in HaCaT cells. In contrast, transient expression of mutant loricrin in HaCaT keratinocytes does not result in PCD or activation of casapse-14. The number of PCD cells in cells transfected with WT loricrin was markedly higher than that in cells of transfected mock or mutant loricrin. In addition, we showed positive TUNEL staining in WT loricrin-transfected cells. Although we demonstrated that PCD occurred in the HaCaT cells after transient transfection of WT loricrin, we assume that this response represents a tissue-specific form of PCD that differs from classical apoptosis. The frame-shift mutations in the loricrin gene have produced mutant forms of loricrin with altered and extended COOH termini, as a consequence of alternative, downstream termination signals. Thus, the common feature of all loricrin mutations described to date is replacement of the COOH-terminal Gly- and Gln/Lys-rich domain with highly charged Arg- and Leu-rich domain amino acid sequences. Because the COOH-terminus of mutant loricrin is very different from the WT loricrin, namely, acquiring a nuclear localization signal, mutant loricrin accumulates in the nucleus. Mutant loricrin overexpressed in HaCaT cells by transfection did not cause PCD *in vitro*, which might be related to pathogenesis of

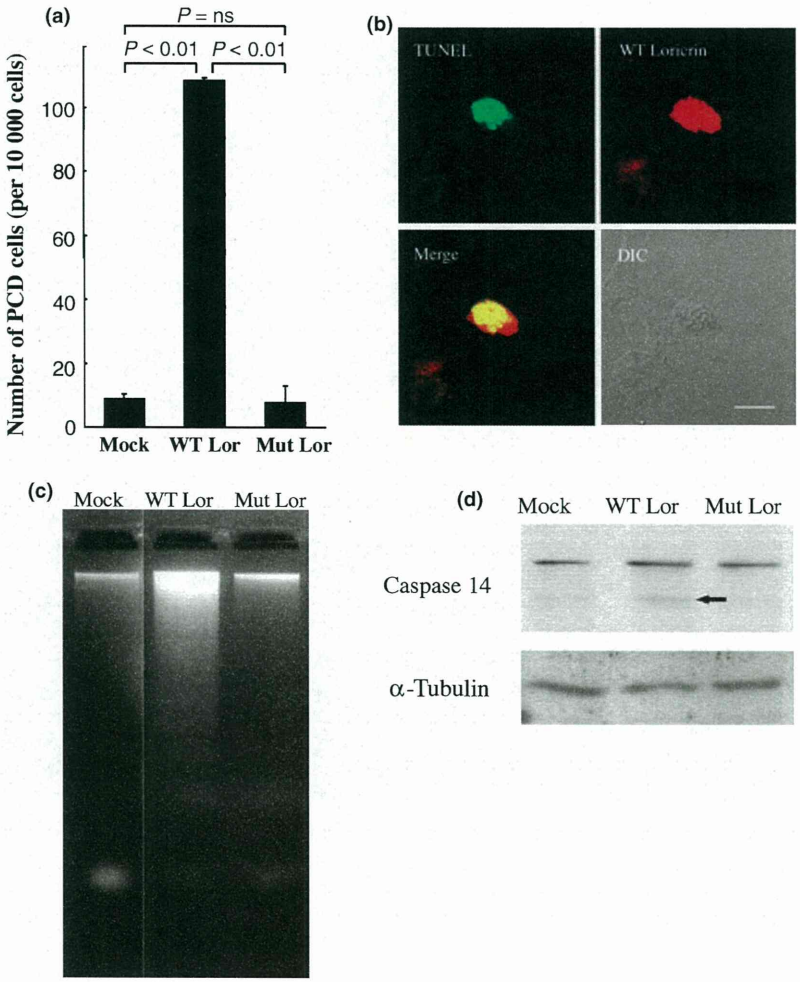

Figure 3. Induction of programmed cell death (PCD) by wild-type (WT) loricrin but not by mutant loricrin. (a) Number of PCD cells was significantly higher in WT loricrin than in mock or mutant loricrin (morphology) (n = 5). Quantification of PCD was performed by both staining PCD nuclei with SYTO 13 and plasma-membrane permeabilization with Trypan blue. (b) Double-stainings with 1:100-diluted anti-V5 antibody (red; upper right panel) and transferase deoxytidyl uridine end labeling (TUNEL) staining (green; upper left panel). Lower left panel shows merge of the two stainings. Positive TUNEL stainings were observed in the nuclei in WT loricrin-transfected cells. (Scale bars: 25 μm.) (c) Data from the DNA fragmentation assay showed that only WT loricrin induced DNA ladders. (d) Activation of caspase-14 by WT loricrin. Immunoblot with 1:5000 diluted anti-caspase-14 and with 1:200 diluted anti-α-tubulin antibody. Caspase-14 was activated in WT loricrin-transfected cells. Similar data were obtained in five experiments. DIC, differential interference contrast.

keratoderma although more studies are needed. Ishida-Yamamoto *et al.*[16] reported that number of TUNEL-positive cells was increased in the skin of loricrin keratoderma. They reported that epidermal differentiation in loricrin keratoderma seemed to be disrupted at the very late stages, immediately before the disintegration of apoptotic nuclei containing profilaggrin amino-terminus. Anti-apoptotic protein, such as Mcl-1, might be expressed more abundantly in HaCaT cells than *in vivo* epidermis because HaCaT cells were spontaneously immortalized an aneuploid human keratinocyte cell line.[24]

Filaggrin is an intermediate filament-associated protein that aggregates epidermal keratin filaments *in vitro* and is thought to perform a similar function during terminal differentiation *in vivo*. Loricrin and filaggrin are two major proteins expressed by terminally differentiated epidermal keratinocytes. Recently,

the importance of filaggrin has been underscored by demonstrating that loss-of-function mutations in the profilaggrin gene underlie the skin disease ichthyosis vulgaris, and that they strongly predispose to atopic dermatitis and asthma.[25,26] Dale *et al.*[27] showed that transient expression of filaggrin in epithelial cells led cell contraction, nuclear membrane breakdown and nuclear condensation. Dale *et al.*[27] and Kuechle *et al.*[28] stated that a low transfection rate is also seen in filaggrin constructs (<2%) as we observed with WT and mutant loricrin constructs. They reported that green fluorescent protein (GFP) and β-galactosidase control constructs showed 15–20% transfection rate. We also observed that the transfection rate of pcDNA3.1/V5-His WT keratin 14 was 20–30%. We also tried Lipofectamine 2000 (Invitrogen) as a transfection reagent. However, transfection efficiency of loricrin was almost the same as using LipofectAMINE plus reagent (Invitrogen). The reason why there is disparity in transfection rate between loricrin and keratin 14 constructs is not currently clear. In addition, we could not detect proteins by immunoblot analysis after transfection of WT and mutant loricrin constructs into cultured normal human epidermal keratinocytes. Similarly, we observed a cystatin A expression vector with cytomegalovirus immediate early promoter could not transfect cystatin A in cultured normal human epidermal keratinocytes.[29] Transfection of cornified cell envelope component proteins such as loricrin, filaggrin or cystatin A into cultured keratinocytes may be very difficult.

We formerly showed that no alterations could be observed in mice with an approximately twofold overexpression of human WT loricrin.[3] We also observed that human cystatin A transgenic mice did not show any abnormalities in the epidermis or hair follicle.[29] Presland *et al.*[30] created human filaggrin transgenic mice and observed no abnormalities in the epidermis, hair structures or tissue organization. Interestingly enough, there was no evidence of altered keratin filament organization in the suprabasal layers of filaggrin transgenic epidermis. On the contrary to these transgenic mice *in vivo* data, we observed that WT loricrin-transfected HaCaT keratinocytes were susceptible to PCD. Dale *et al.*[27] proved that transient transfection of epidermal filaggrin efficiently aggregates keratin filaments when expressed *in vitro* either in rat keratinocytes (keratin5/keratin14 and keratin1/keratin10) or monkey COS-7 cells (keratin8/keratin18). Presland *et al.*[30,31] reported that there was a disruption of cell–cell adhesion in keratinocytes overexpressing filaggrin, which they did not observe in transgenic mice overexpressing filaggrin. They speculated that cultured cells might be more sensitive to keratin filament disruption than epidermal tissue, which expressed a greater diversity of keratin proteins and thus contained a more robust intermediate filament network with stronger cell–cell adhesion through desmosomes. Similarly, we think cultured HaCaT cells may be more sensitive to various PCD stimuli than *in vivo* epidermal tissue which express a greater diversity of keratin proteins and contain an abundant type I keratin proteins that are known to prevent apoptosis.

Although the bulk of WT loricrin exists within keratohyalin granules and cornified cell envelope, WT loricrin is also known to be present in the nucleus at *in vivo* epidermis.[4] We also confirm that WT loricrin distributes in the nucleus *in vitro* transfected HaCaT cells. However, the function of WT loricrin is not known yet. The profilaggrin N-terminal domain localizes to both cytoplasm and nucleus of epidermal granular layer cells. Profilaggrin is a large phosphoprotein that is expressed in the granular cells of epidermis where it is localized in keratohyalin. It consists of multiple copies of single filaggrin units plus N- and C-terminal sequences that differ from filaggrin. The N-terminal sequence of human profilaggrin comprises two distinct domains; an acidic A domain of 81 amino acids that binds calcium, and a cationic B domain of 212 residues. The cellular distribution of WT loricrin is similar to that of profilaggrin N-terminal domain. We speculate that WT loricrin may interact with profilaggrin N-terminal domain *in vivo* and that this interaction may have some role in normal epidermal keratinization. To explore the expression of nuclear WT loricrin in cultured keratinocytes and epidermis and examine its association with profilaggrin N-terminal domain would be of great interest as a future project.

In summary, this study shows that expression of WT loricrin in HaCaT keratinocytes causes PCD whereas mutant loricrin is unable to cause PCD. Our results may implicate novel function of WT loricrin considering that the overexpression of filaggrin and profilaggrin results in PCD in both simple epithelial cells (COS-7) and rat epidermal keratinocyte cell line (REK).[27]

ACKNOWLEDGMENTS

We are grateful to Dr N. Fusenig for HaCaT cells; F. Naruse, T. Takamura and F. Nishiyama for technical assistance and artwork. This work was in part supported by grants from the Ministries of Health, Labor and Welfare and Education, Culture, Sports, Science, and Technology of Japan.

REFERENCES

1 Yoneda K, Hohl D, McBride OW *et al.* The human loricrin gene. *J Biol Chem* 1992; **267**: 18060–18066.
2 Yoneda K, McBride OW, Korge BP, Kim IG, Steinert PM. The cornified cell envelope: loricrin and transglutaminases. *J Dermatol* 1992; **19**: 761–764.
3 Yoneda K, Steinert PM. Overexpression of human loricrin in transgenic mice produces a normal phenotype. *Proc Natl Acad Sci USA* 1993; **90**: 10754–10758.
4 Ishida-Yamamoto A, Hohl D, Roop DR, Iizuka H, Eady RA. Loricrin immunoreactivity in human skin: localization to specific granules (L-granules) in acrosyringia. *Arch Dermatol Res* 1993; **285**: 491–498.
5 Ishida-Yamamoto A. Loricrin keratoderma: a novel disease entity characterized by nuclear accumulation of mutant loricrin. *J Dermatol Sci* 2003; **31**: 3–8.
6 Bickenbach JR, Greer JM, Bundman DS, Rothnagel JA, Roop DR. Loricrin expression is coordinated with other epidermal proteins and the appearance of lipid lamellar granules in development. *J Invest Dermatol* 1995; **104**: 405–410.
7 Maestrini E, Monaco AP, McGrath JA *et al.* A molecular defect in loricrin, the major component of the cornified cell envelope, underlies Vohwinkel's syndrome. *Nat Genet* 1996; **13**: 70–77.
8 Korge BP, Ishida-Yamamoto A, Punter C *et al.* Loricrin mutation in Vohwinkel's keratoderma is unique to the variant with ichthyosis. *J Invest Dermatol* 1997; **109**: 604–610.
9 Armstrong DK, McKenna KE, Hughes AE. A novel insertional mutation in loricrin in Vohwinkel's Keratoderma. *J Invest Dermatol* 1998; **111**: 702–704.
10 Takahashi H, Ishida-Yamamoto A, Kishi A, Ohara K, Iizuka H. Loricrin gene mutation in a Japanese patient of Vohwinkel's syndrome. *J Dermatol Sci* 1999; **19**: 44–47.
11 Matsumoto K, Muto M, Seki S *et al.* Loricrin keratoderma: a cause of congenital ichthyosiform erythroderma and collodion baby. *Br J Dermatol* 2001; **145**: 657–660.
12 O'Driscoll J, Muston GC, McGrath JA, Lam HM, Ashworth J, Christiano AM. A recurrent mutation in the loricrin gene underlies the ichthyotic variant of Vohwinkel syndrome. *Clin Exp Dermatol* 2002; **27**: 243–246.
13 Gedicke MM, Traupe H, Fischer B, Tinschert S, Hennies HC. Towards characterization of palmoplantar keratoderma caused by gain-of-function mutation in loricrin: analysis of a family and review of the literature. *Br J Dermatol* 2006; **154**: 167–171.
14 Ishida-Yamamoto A, McGrath JA, Lam H, Iizuka H, Friedman RA, Christiano AM. The molecular pathology of progressive symmetric erythrokeratoderma: a frameshift mutation in the loricrin gene and perturbations in the cornified cell envelope. *Am J Hum Genet* 1997; **61**: 581–589.
15 Ishida-Yamamoto A, Takahashi H, Iizuka H. Loricrin and human skin diseases: molecular basis of loricrin keratodermas. *Histol Histopathol* 1998; **13**: 819–826.
16 Ishida-Yamamoto A, Takahashi H, Presland RB, Dale BA, Iizuka H. Translocation of profilaggrin N-terminal domain into keratinocyte nuclei with fragmented DNA in normal human skin and loricrin keratoderma. *Lab Invest* 1998; **78**: 1245–1253.
17 Song S, Shen C, Song G *et al.* A novel c.545-546insG mutation in the loricrin gene correlates with a heterogeneous phenotype of loricrin keratoderma. *Br J Dermatol* 2008; **159**: 714–719.
18 Yoneda K, Furukawa T, Zheng YJ *et al.* An autocrine/paracrine loop linking keratin 14 aggregates to tumor necrosis factor alpha-mediated cytotoxicity in a keratinocyte model of epidermolysis bullosa simplex. *J Biol Chem* 2004; **279**: 7296–7303.
19 Inoue T, Yoneda K, Manabe M, Demitsu T. Spontaneous regression of merkel cell carcinoma: a comparative study of TUNEL index and tumor-infiltrating lymphocytes between spontaneous regression and non-regression group. *J Dermatol Sci* 2000; **24**: 203–211.
20 Yoneda K, Fujimoto T, Imamura S, Ogawa K. Distribution of fodrin in the keratinocyte *in vivo* and *in vitro*. *J Invest Dermatol* 1990; **94**: 724–729.
21 Ishida-Yamamoto A, Kato H, Kiyama H *et al.* Mutant loricrin is not crosslinked into the cornified cell envelope but is translocated into the nucleus in loricrin keratoderma. *J Invest Dermatol* 2000; **115**: 1088–1094.
22 DiColandrea T, Karashima T, Maatta A, Watt FM. Subcellular distribution of envoplakin and periplakin: insights into their role as precursors of the epidermal cornified envelope. *J Cell Biol* 2000; **151**: 573–586.
23 Boukamp P, Petrussevska RT, Breitkreutz D, Hornung J, Markham A, Fusenig NE. Normal keratinization in a spontaneously immortalized aneuploid human keratinocyte cell line. *J Cell Biol* 1988; **106**: 761–771.
24 Sitailo LA, Jerome-Morais A, Denning MF. Mcl-1 functions as major epidermal survival protein required for proper kertinocyte differentiation. *J Invest Dermatol* 2009; **129**: 1351–1360.

25 Smith FJ, Irvine AD, Terron-Kwiatkowski A *et al.* Loss-of-function mutations in the gene encoding filaggrin cause ichthyosis vulgaris. *Nat Genet* 2006; **38**: 337–342.
26 Palmer CN, Irvine AD, Terron-Kwiatkowski A *et al.* Common loss-of-function variants of the epidermal barrier protein filaggrin are a major predisposing factor for atopic dermatitis. *Nat Genet* 2006; **38**: 441–446.
27 Dale BA, Presland RB, Lewis SP, Underwood RA, Fleckman P. Transient expression of epidermal filaggrin in cultured cells causes collapse of intermediate filament networks with alteration of cell shape and nuclear integrity. *J Invest Dermatol* 1997; **108**: 179–187.
28 Kuechle MK, Presland RB, Lewis SP, Fleckman P, Dale BA. Inducible expression of filaggrin increases keratinocyte susceptibility to apoptotic cell death. *Cell Death Differ* 2000; **7**: 566–573.
29 Takahashi H, Komatsu N, Ibe M, Ishida-Yamamoto A, Hashimoto Y, Iizuka H. Cystatin A suppresses ultraviolet B-induced apoptosis of keratinocytes. *J Dermatol Sci* 2007; **46**: 179–187.
30 Presland RB, Coulombe PA, Eckert RL, Mao-Qiang M, Feingold KR, Elias PM. Barrier function in transgenic mice overexpressing K16, involucrin, and filaggrin in the suprabasal epidermis. *J Invest Dermatol* 2004; **123**: 603–606.
31 Presland RB, Kuechle MK, Lewis SP, Fleckman P, Dale BA. Regulated expression of human filaggrin in keratinocytes results in cytoskeletal disruption, loss of cell-cell adhesion, and cell cycle arrest. *Exp Cell Res* 2001; **270**: 199–213.

Pediatric Diabetes

ISPAD International Society for Pediatric and Adolescent Diabetes

Pediatric Diabetes 2012: 13: 26–32
doi: 10.1111/j.1399-5448.2011.00827.x

Pediatric Diabetes

Original Article

Comprehensive molecular analysis of Japanese patients with pediatric-onset MODY-type diabetes mellitus

Yorifuji T, Fujimaru R, Hosokawa Y, Tamagawa N, Shiozaki M, Aizu K, Jinno K, Maruo Y, Nagasaka H, Tajima T, Kobayashi K, Urakami T. Comprehensive molecular analysis of Japanese patients with pediatric-onset MODY-type diabetes mellitus.
Pediatric Diabetes 2012: 13: 26–32.

Background: In Asians, mutations in the known maturity-onset diabetes of the young (MODY) genes have been identified in only <15% of patients. These results were obtained mostly through studies on adult patients.
Objective: To investigate the molecular basis of Japanese patients with pediatric-onset MODY-type diabetes.
Subjects: Eighty Japanese patients with pediatric-onset MODY-type diabetes.
Methods: Mitochondrial 3243A>G mutation was first tested by the polymerase chain reaction restriction fragment length polymorphism analysis for maternally inherited families. Then, all coding exons and exon–intron boundaries of the *HNF1A*, *HNF1B*, *GCK*, and *HNF4A* genes were amplified from genomic DNA and directly sequenced. Multiplex ligation-dependent probe amplification analysis was also performed to detect whole-exon deletions.
Results: After excluding one patient with a mitochondrial 3243A>G, mutations were identified in 38 (48.1%) patients; 18 had *GCK* mutations, 11 had *HNF1A* mutations, 3 had *HNF4A* mutations, and 6 had *HNF1B* mutations. In patients aged <8 yr, mutations were detected mostly in *GCK* at a higher frequency (63.6%). In patients >9 yr of age, mutations were identified less frequently (45.1%), with *HNF1A* mutations being the most frequent. A large fraction of mutation-negative patients showed elevated homeostasis model assessment (HOMA) insulin-resistance and normal HOMA-β indices. Most of the *HNF1B* mutations were large deletions, and, interestingly, renal cysts were undetectable in two patients with whole-gene deletion of *HNF1B*.
Conclusion: In Japanese patients with pediatric-onset MODY-type diabetes, mutations in known genes were identified at a much higher frequency than previously reported for adult Asians. A fraction of mutation-negative patients presented with insulin-resistance and normal insulin-secretory capacities resembling early-onset type 2 diabetes.

Tohru Yorifuji[a,b], Rika Fujimaru[a], Yuki Hosokawa[a], Nobuyoshi Tamagawa[b], Momoko Shiozaki[b], Katsuya Aizu[c], Kazuhiko Jinno[d], Yoshihiro Maruo[e], Hironori Nagasaka[f], Toshihiro Tajima[g], Koji Kobayashi[h] and Tatsuhiko Urakami[i]

[a]Department of Pediatric Endocrinology and Metabolism, Children's Medical Center, Osaka City General Hospital, 2-13-22 Miyakojima-Hondori, Miyakojima, Osaka 534-0021, Japan; [b]Clinical Research Center, Osaka City General Hospital, 5-15-21 Nakano, Miyakojima, Osaka 534-0027, Japan; [c]Division of Endocrinology and Metabolism, Saitama Children's Medical Center, 2100 Magome, Iwatsuki, Saitama 339-8551, Japan; [d]Department of Pediatrics, Hiroshima General Hospital of West Japan Railway Company, 3-1-36 Futabanosato, Higashi, Hiroshima 732-0057, Japan; [e]Department of Pediatrics, Shiga University of Medical Science, Seta-Tsukinowa, Otsu, Shiga 520-2192, Japan; [f]Department of Pediatrics, Takarazuka City Hospital, 4-5-1 Obama, Takarazuka, Hyogo 665-0827, Japan; [g]Department of Pediatrics, Hokkaido University School of Medicine, Kita 14, Nishi 5, Kita, Sapporo 060-8648, Japan; [h]Department of Pediatrics, Yamanashi Kosei Hospital, 860 Ochiai, Yamanashi, Yamanashi 405-0033, Japan; and [i]Department of Pediatrics, Nihon University School of Medicine, 1-8-13 Kanda Surugadai, Chiyoda, Tokyo 101-8309, Japan

Key words: Japanese – MODY – mutation – pediatric